Supplementary information

Ferroelectric ZrO_2 phases from Infrared spectroscopy

Ali El Boutaybi[a], Rebecca, Cervasio[b], Alban Degezelle[a], Thomas Maroutian[a],
Jean-Blaise Brubach[b], Valérie Demange[c], Ludovic Largeau[a], Marine Verseils[b], Sylvia
Matzen[a], Guillaume Agnus[a], Laurent Vivien[a], Panagiotis Karamanis[d], Michel Rérat[d],
Pascale Roy[b], and Philippe Lecoeur[a]

[a]Centre de Nanosciences et de Nanotechnologies (C2N), Universite Paris-Saclay, CNRS,
91120 Palaiseau, France
[b]Synchrotron SOLEIL - CNRS - CEA Paris-Saclay, 91120 Palaiseau, France
[c]ISCR Univ Rennes, CNRS, ISCR—UMR 6226, ScanMAT—UMS 2001, Rennes, France
[d]Université de Pau et des Pays de l'Adour, CNRS, IPREM, E2S UPPA, Pau, France
ali.el-boutaybi@c2n.upsaclay.fr

1 IR active modes

As mentioned in the main paper, first-principles calculations suggest the stability of other polar phases, including the Pc and $Pmn2_1$ phases. Although these phases have not been observed experimentally yet, the Pc phase was found to have low bulk energy, similar to the $Pbc2_1$ phase in HfO_2 and ZrO_2 [1], while the $Pmn2_1$ phase was found to have lower energy than the t phase in HfO_2 [1, 2], and higher energy in ZrO_2 [1]. These two polar phases are also considered here. To investigate their IR activities and absorbance, unit cells of 6 and 24 atoms were used for $Pmn2_1$ and Pc, respectively [1, 3]. The simulated IR absorbance and peak positions are presented in Figure S1.d for the $Pmn2_1$ phase, displaying six bands located at 148, 244, 326, 468, 605, and 712 cm^{-1}, with three bands showing close response to the t phase, mainly the ones at 148, 326, and 468 cm^{-1}. However, the gap between the bands at 326 cm^{-1} and 468 cm^{-1} is higher for the $Pmn2_1$ phase compared to the t phase (around 142 cm^{-1} Vs. 93 cm^{-1}), and also the intensity ratio between the lower bands (148 and 326 cm^{-1}) differs in the two phases (see Figures S1.d and 1.b in main paper).
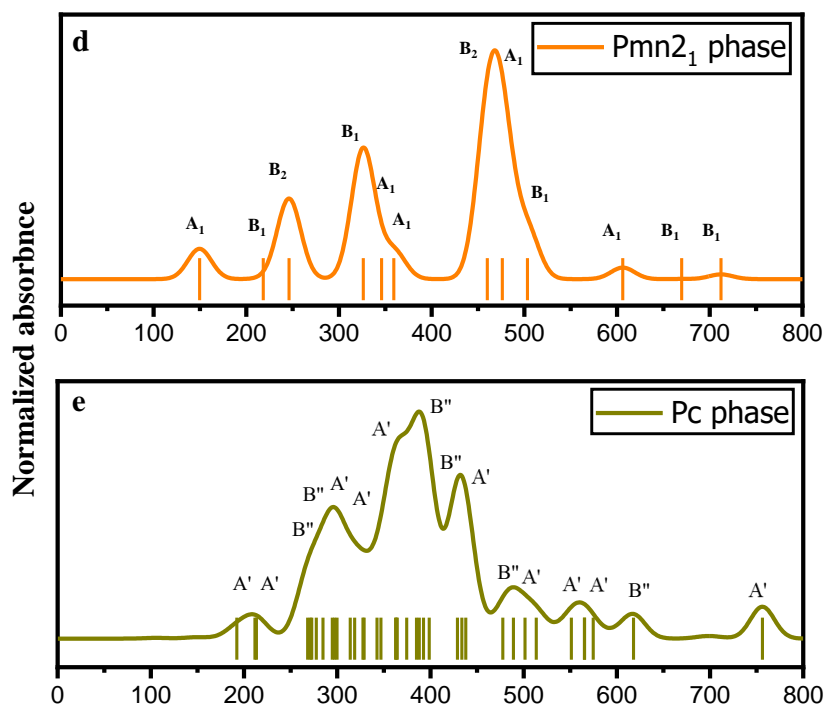

Figure S1: Infrared absorbance responses of ZrO_2 for the polar $Pmn2_1$ and Pc phases. All IR active modes are highlighted in bar form, with emphasis on the modes contributing most to IR absorbance. Only the high-intensity modes in IR are shown for the polar Pc phase since this phase was computed with a 24-atom unit cell and has a high number of IR modes (69 modes, see Tables S1 and S2 below).

Furthermore, the Pc phase with 24 atoms in the unit cell gives 72 phonon modes, and the 69 optical phonon modes are all active in IR. Even though this phase has a high number of IR active modes, only a few are intense and contribute to the IR absorbance as shown in Figure S1.e. The IR absorbance spectrum in the range between 300-500 cm^{-1} is close to the one of the Pbc2$_1$ phase (see the main paper), with the main intense peak located at around 400 cm^{-1} for both phases (390 cm^{-1} for Pc phase Vs. 400 cm^{-1} for Pbc2$_1$ phase). The distinctive IR band for Pc phase results from four phonon modes (B$''$ at 285 cm^{-1}, B$''$ at 295 cm^{-1}, A$'$ at 297 cm^{-1}, and A$'$ at 299 cm^{-1}) and is located at around 295 cm^{-1}. Also, the response at around 488 cm^{-1}, which is a result of the modes A$'$ at 478 cm^{-1}, B$''$ at 489 cm^{-1}, and B$''$ at 502 cm^{-1}, is only intense in Pc phase compared to other polar phases even though a similar band is also present in the non-polar m phase (see the main paper and tables S1 and S2). However, m phase can be distinguished by XRD analysis.

In the following pages, Tables S1 and S2 display all IR active modes for the 6 investigated phases: Polar Pbc21, R3m, Pmn21, and Pc phases, and non-polar t and m phases. The evaluated IR intensities are also shown.

Table S1: IR-active modes for the t, Pbc2$_1$, and R3m phases of ZrO$_2$, with their corresponding intensities (in km/mol) evaluated using the CRYSTAL code and B3LYP functional.

t-ZrO$_2$			Pbc2$_1$-ZrO$_2$			R3m-ZrO$_2$		
mode	cm^{-1}	I	mode	cm^{-1}	I	mode	cm^{-1}	I
E$_u$	138	1921	A$_1$	102	333	E	76	0.10
A$_{2u}$	333	2128	B$_2$	165	3.00	E	167	3.04
E$_u$	426	3562	A$_1$	186	163	A$_1$	170	1.44
			B$_1$	187	549	E	174	0.10
			B$_1$	224	1202	A$_1$	221	1785
			B$_2$	233	956	E	233	3346
			B$_2$	289	51	A$_1$	268	0.48
			A$_1$	291	80	E	324	31
			B$_1$	298	60	A$_1$	353	1715
			A$_1$	316	1927	E	358	3423
			B$_1$	329	512	A$_1$	450	1559
			B$_2$	345	2041	E	457	3606
			A$_1$	351	57	A$_1$	533	87
			B$_1$	387	442	E	536	262
			B$_2$	399	1356	E	587	1.12
			B$_1$	402	2929	A$_1$	674	35
			A$_1$	445	1924	E	683	88
			B$_2$	460	284	E	720	0.30
			B$_1$	514	396	A$_1$	755	1.21
			B$_1$	545	18			
			A$_1$	566	96			
			B$_2$	621	92			
			B$_2$	683	22			
			B$_1$	726	353			

Table S2: IR-active modes for the Pmn2_1, m(P2_1/c), and Pc phases of ZrO$_2$, with their corresponding intensities (in km/mol) evaluated using the CRYSTAL code and B3LYP functional.

\multicolumn{3}{c}{Pmn2_1-ZrO$_2$}	\multicolumn{3}{c}{m(P2_1/c)-ZrO$_2$}	\multicolumn{3}{c}{Pc-ZrO$_2$}
cm^{-1}	mode	I	cm^{-1}	mode	I	cm^{-1}	mode	I
149	A_1	365	199	A_u	19	106	A'	20.19
218	B_2	6.28	243	B_u	671	138	B"	0.02
246	B_1	972	255	A_u	120	148	A'	26.61
326	B_2	1575	277	A_u	842	153	A'	13.17
345	A_1	6.05	323	B_u	660	158	B"	0.03
359	A_1	336	335	B_u	2754	186	B"	4.16
460	B_1	1712	370	A_u	1072	192	A'	288
476	A_1	1650	371	B_u	2126	197	B"	9.76
503	B_2	573	425	A_u	2025	199	B"	9.32
606	A_1	139	438	B_u	1425	205	B"	1.38
669	B_2	2.49	503	A_u	906	212	A'	220
712	B_2	57	533	B_u	1195	213	A'	345
			601	A_u	668	227	B"	0.26
			675	A_u	12	236	A'	2.67
			752	B_u	616	268	A	1183
						271	B"	430
						272	A'	107
						277	A'	40.07
						284	B"	514
						294	B"	1242
						297	A'	1098
						299	A'	454
						314	B"	292
						318	A'	1050
						327	B"	34.47
						327	A'	332
						328	A'	446
						342	B"	321
						346	A'	917
						362	A'	1850
						363	B"	151
						364	A'	2252
						374	B"	180
						383	A'	19.18
						384	B"	355
						388	A'	2020
						392	B"	2697

398	A'	855
408	A'	31.93
411	B"	29.07
428	B"	1687
433	A'	2306
438	B"	626
455	A'	79.90
477	A'	499.
488	B"	877
501	B"	189
505	B"	0.33
513	A'	649
538	B"	38.52
551	A'	529
565	A'	431
565	B"	116
575	A'	154
581	B"	2.68
596	A'	56.87
604	B"	49.56
606	B"	2.18
618	B"	647
646	A'	1.71
657	B"	0.07 A
697	B"	56.95
700	A'	3.75
706	B"	14.90
719	B"	1.21
756	A'	889
785	B"	0.20

2 R3m phase and intermediate P1 phase

Figure S2.a depicts the infrared absorbance response of the R3m phase stabilized under pressure (using the experimental volume), as discussed in the main paper, while the R3m symmetry was maintained, and compares it to the one for the (unstable) R3m phase at the optimized volume. Both IR responses are quite similar, with a shift to lower energy for the peaks of the R3m phase at the optimized volume. This similarity arises because the unstable modes correspond to the first optical modes (E), which do not significantly contribute to the IR absorbance of the R3m ZrO_2 phase.
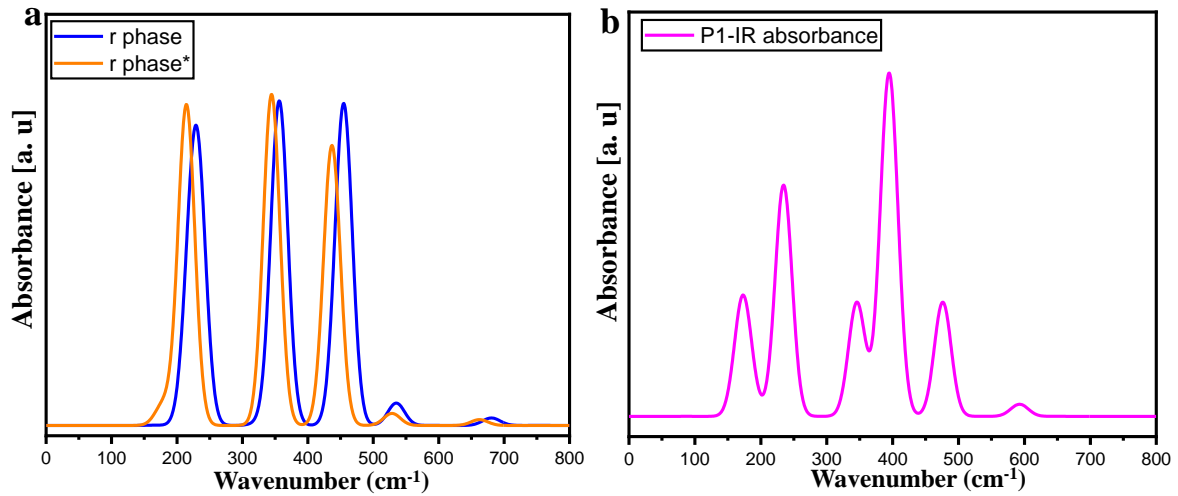
Figure S2: (a) IR absorbance response of ZrO_2 R3m phase (blue). The IR absorbance computed at optimized volume (r phase*, orange) for the R3m phase is also shown for comparison. (b) IR absorbance of the intermediate phase P1 discussed in the main paper.

The IR absorbance of the intermediate phase identified in the main paper with the triclinic space group P1 was also calculated and is presented in Figure S2.b. It is evident that this intermediate phase exhibits a much richer set of IR bands, as is expected for the triclinic crystal system. Note that this intermediate phase is unstable; hence, a constant pressure was applied in order to obtain only positive phonons and calculate the IR absorbance.

Table S3 presents the lattice parameters of the P1 intermediate phase discussed in the main paper. It should be noted that this phase is unstable, characterized by the presence of the unstable B" phonon mode.

Table S3: Atomic positions and lattice parameters of the intermediate P1 phase.

	a(Å)	b(Å)	c(Å)
	5.15812746	5.15812746	5.13569359
	x/a	y/b	z/c
Zr1	8.427491865210E-02	-4.157444327672E-01	8.422283571494E-02
Zr2	8.430258783145E-02	8.430258783132E-02	-4.157410223418E-01
Zr3	-4.157444327669E-01	8.427491865178E-02	8.422283571493E-02
Zr4	-4.156909592185E-01	-4.156909592195E-01	-4.158471357902E-01
O1	3.101728904277E-01	-1.416928197962E-01	3.310715204873E-01
O2	3.100846754547E-01	3.100846754551E-01	-1.624213398556E-01
O3	-1.416928197965E-01	3.101728904279E-01	3.310715204873E-01
O4	-1.899479774715E-01	3.584818991351E-01	-1.622246433052E-01
O5	-1.898684734175E-01	-1.898684734176E-01	3.308084446862E-01
O6	3.584818991349E-01	-1.899479774714E-01	-1.622246433052E-01
O7	-1.415695536503E-01	-1.415695536506E-01	-1.625545369866E-01
O8	3.583247203773E-01	3.583247203781E-01	3.309612133794E-01

3 Strain effect on IR absorbance spectra of t and R3m phases

Figure S3 depicts the IR absorbance spectra of symmetrized and non-symmetrized ZrO_2 t phase. Removing the symmetry activates additional IR bands; however, the intensities of these new IR bands are almost zero, as depicted in Figure S3.b.
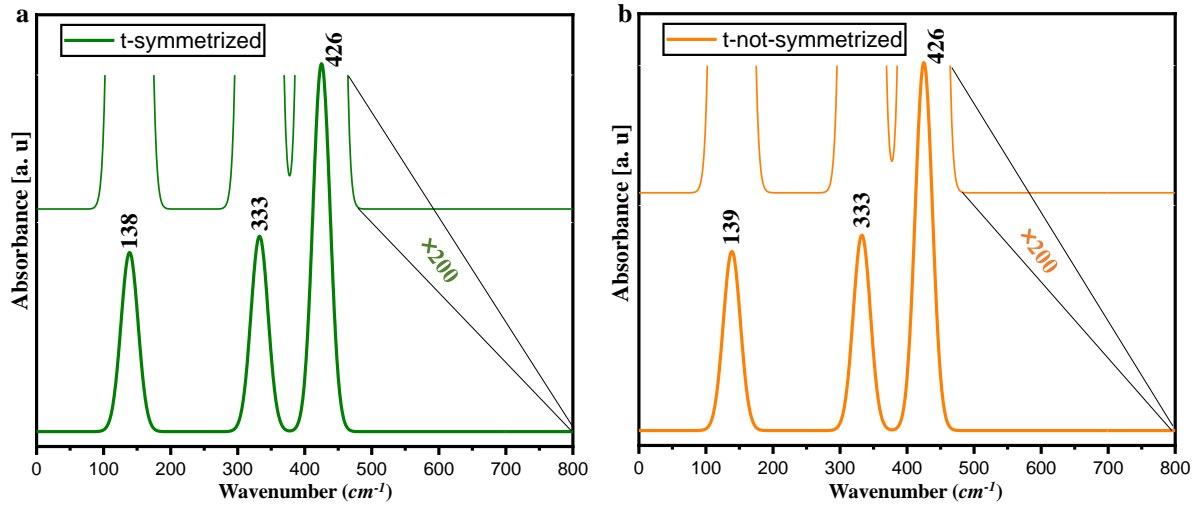

Figure S3: Infrared absorbance responses of ZrO_2 t phase in two cases: (a) with preserved symmetry and (b) with symmetry removed.
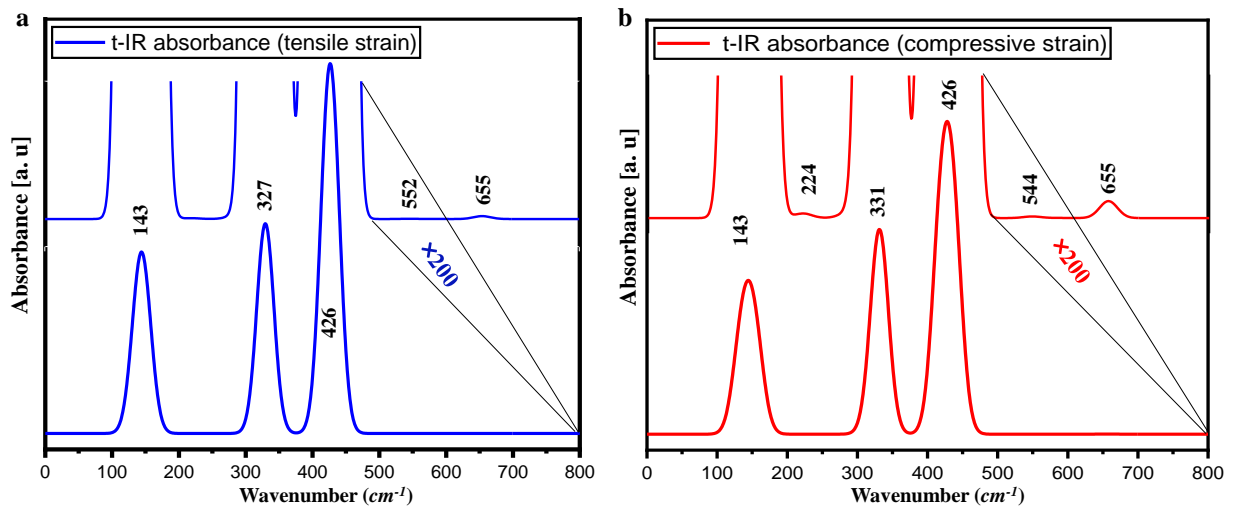

Figure S4: Infrared absorbance responses of ZrO_2 t phase with symmetry removed and submitted to (a) 1% tensile strain and (b) 1% compressive strain.

Now, when applying additional strain (compressive or tensile), the activated IR bands in the non-symmetrized t phase become more pronounced, although the change is relatively small. A zoomed-in portion is shown in Figure S4, where it is evident that these newly activated bands are amplified. Note that the zoomed-in parts shown in Figures S3 and S4 have the same intensity scale for comparison. The tensile strain of 1% (Figure S4.a) caused a shift of the lowest band from around 138 cm^{-1} to 143 cm^{-1}, and the additional IR bands are located at 552 cm^{-1} and 655 cm^{-1}.

Regarding the compressive strain of 1% (Figure S4.b), a similar effect as for tensile strain is observed, particularly for the lowest energy IR band. However, the compressive strain appears to amplify the additional IR bands to a greater intensity compared to tensile strain, as shown in Figure S4. Note that compressive and tensile strains are applied to the unit cell of ZrO_2, considering the (111)-oriented thin films. As a result, in the case of a pseudo-cubic system, the unit cell angle will be distorted. Under compressive strain, the unit cell angle will be below 90°, while under tensile strain, it will be above 90°.

In the case of the r phase, which is obtained when compressive strain is applied, the IR absorbance is computed at two different strain values. The first is the strain reported experimentally in ZrO_2 with a rhombohedral angle of 89.56° and discussed in the main paper, and the second is the compressive strain applied with a rhombohedral angle of 89°. The IR absorbance responses are shown in Figure S5.

Under high compressive strain (Figure S5.b), the lowest IR absorbance band is more significantly affected. It becomes broader and decreases in intensity compared to the same band shown in Figure S5.a. The remaining IR bands, however, undergo minimal changes, with shifts of less than +/- 5 cm^{-1}.

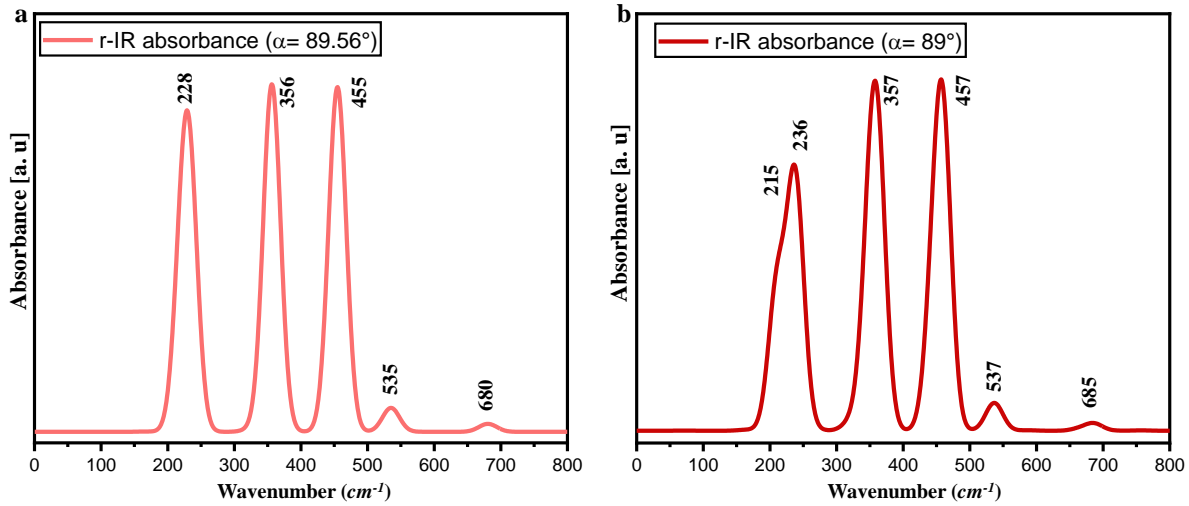Figure S5: Infrared absorbance responses of the ZrO_2 r phase under two different compressive strains.

4 Cm phase

The ZrO$_2$ Cm phase was identified by following the unstable phonon mode in the R3m phase. This phase belongs to the monoclinic structure with space group Cm (No.8). The atomic positions are provided in the table below. It is worth noting that this structure can be represented in two different forms, rhombohedral or monoclinic.

Table S4: Atomic positions and lattice parameters of Cm phase in monoclinic representation.

	a(Å)	b(Å)	c(Å)
	7.265995	7.265995	5.205750
	x/a	y/b	z/c
Zr1	-0.165833	-0.250028	0.084284
Zr2	0.084451	0.000000	-0.415768
Zr3	-0.415589	0.000000	-0.415768
O1	0.084299	-0.249866	0.293945
O2	0.334004	0.000000	-0.125603
O3	0.084260	0.250112	-0.206018
O4	-0.165802	0.000000	0.374661
O5	-0.165611	0.000000	-0.125381
O6	0.334374	0.000000	0.374428
Angles	α	β	γ
	90	90.05	90

Figure S6 displays the IR absorbance of the Cm phase, which, at first glance, appears similar to that of the t phase (Figure S3.a). However, there is a noticeable shift in the band around 333 cm^{-1} in the Cm phase. Moreover, small additional bands are observed at around 215 cm^{-1} and 279 cm^{-1}. These observations suggest that the Cm phase IR absorbance response should exhibit similar behavior with strain as the t phase, discussed in the previous section (Figure S4).
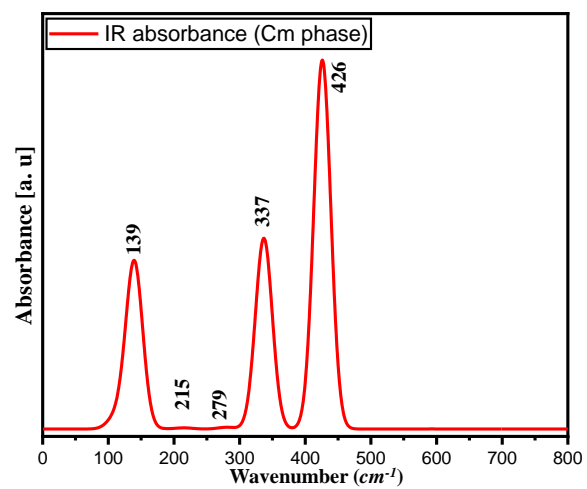
Figure S6: Infrared absorbance response of the ZrO$_2$ Cm phase.

References

[1] L. Azevedo Antunes, R. Ganser, C. Kuenneth, and A. Kersch, "Characteristics of low-energy phases of hafnia and zirconia from density functional theory calculations", physica status solidi (RRL) – Rapid Research Letters **16**, 2100636 (2022).

[2] Y. Qi, S. Singh, C. Lau, F.-T. Huang, X. Xu, F. J. Walker, C. H. Ahn, S.-W. Cheong, and K. M. Rabe, "Stabilization of competing ferroelectric phases of HfO_2 under epitaxial strain", Phys. Rev. Lett. **125**, 257603 (2020).

[3] T. D. Huan, V. Sharma, G. A. Rossetti, and R. Ramprasad, "Pathways towards ferroelectricity in hafnia", Phys. Rev. B **90**, 064111 (2014).